

INVERSE DETERMINATION OF THERMAL PARAMETERS OF SOLID PROPELLANTS FOR MATHEMATICAL MODELS IN COOK-OFF SIMULATIONS USING SMALL SAMPLE QUANTITIES

Daniel Tomaschewski, Christian Teicht

Fraunhofer Institute for Chemical Technology ICT

Joseph-von-Fraunhofer Straße 7, 76327 Pfinztal, Germany

ABSTRACT

Understanding the sensitivity of ammunition to external mechanical and thermal stimuli is critical for the safe and effective design of solid propellants in barreled weapon systems. In high-rate-of-fire scenarios, accumulated thermal loading, especially within the barrel, can expose subsequent rounds to elevated temperatures, potentially triggering cook-off through hotspot ignition. Numerical simulations are instrumental in modeling these thermal effects and guiding the design process. State-of-the-art multiphase models can capture the interaction between solid propellants and the gaseous phase in the heating, ignition and combustion processes. However, the predictive accuracy of these models heavily depends on the proper parametrization of thermal transport phenomena within the energy equation. This study presents a simulation based inverse parameter identification methodology to estimate key thermal properties based on small-scale experiments. The resulting parameters can improve the fidelity of thermal simulations and inform future designs aimed at increasing the thermal insensitivity of ammunition systems.

INTRODUCTION

Thermal exposure of ammunition during sustained firing imposes significant risk for cook-off events in solid propellant beds, driven by the formation of hotspots where local heat accumulation exceeds safe thresholds. Insensitive munition (IM) requirements, codified in STANAG 4439 [1] and tested under fast and slow cook-off procedures (STANAG 4240 [2] and STANAG 4382 [3]), motivate the development of numerical tools capable of predicting pre-ignition thermal fields in realistic bed geometries. Multiphase modelling frameworks, which represent the coupled solid propellant and gaseous pore space, are well positioned to simulate conduction, convection, and radiation during heating, ignition, and combustion [4–9].

Predictive success in these frameworks depends on accurate parameterization of energy transport. Thermal conductivity determines the rate at which heat diffuses through individual grains and across contact networks, controlling both the magnitude and distribution of temperature gradients. Radiative heat transfer within the interstitial pores becomes increasingly relevant at elevated temperatures, altering heat fluxes and intensifying local heating beyond conductive expectations. Effective properties that reflect the combined influence of microstructure, material emissivity, and pore geometry are necessary to capture these processes at the bed scale. However, direct acquisition of such properties is constrained by safety, material availability, and the complexity of pore-scale measurement, leading to broad uncertainties in model inputs.

To overcome these constraints, this work establishes a simulation-based inverse parameter identification methodology grounded in small-scale experiments. The approach designs controlled thermal loading scenarios on limited material quantities, records temperature responses with sufficient temporal and spatial resolution, and fits a forward heat transfer model to extract effective thermal conductivity and radiative transfer parameters. The resulting properties are formulated for the energy equation in multiphase simulations, enabling improved representation of heat transport pathways under cook-off-relevant conditions. This inversion strategy emphasizes the reproducibility and transferability of parameters across different heating rates and boundary conditions, aligning the calibration process with IM assessment needs.

By extracting effective thermal parameters from experiments designed for small material quantities, the proposed inversion framework strengthens the fidelity of bed-scale heat-transfer simulations and improves the prediction of hotspot formation under cook-off-relevant conditions. The method bridges laboratory measurements and high-fidelity multiphase models by delivering parameters that are transferable across heating rates and boundary conditions. In doing so, it enables more reliable assessments of thermal sensitivity and supports design decisions on grain geometry, packing density, and material selection that collectively reduce cook-off susceptibility.

EXPERIMENTAL SETUP

A single solid-propellant grain is seated on a monolithic aluminum fixture that serves as both thermal actuator and reference body. The fixture (Figure 1) accommodates two cartridge heaters and two embedded temperature sensors at distinct locations, enabling temperature-controlled operation and independent monitoring of the fixture response. A shallow pedestal on the top surface provides a repeatable seating position for the grain and minimizes lateral motion. Exposed surfaces exchange heat predominantly by thermal radiation with the laboratory environment. Free convection is suppressed by a custom 3D-printed housing lined with thermal insulation, which reduces drafts and limits air heating in the measurement volume; accordingly, external heat exchange is dominated by radiation from the propellant surface. Heat transfer across the grain–fixture interface is imperfect due to microscopic roughness and partial contact, producing a finite interfacial conductance identified in the inversion.

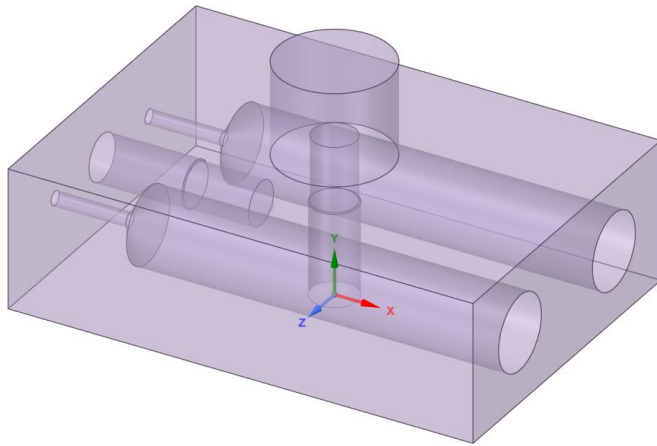


Figure 1: CAD of the fixture.



Figure 2: Propellant grain placed on the insulated fixture in front of the IR camera.

Surface temperatures of the propellant grain are measured by infrared (IR) thermography (Figure 2). The camera is positioned normal to the grain's upper surface with fixed working distance, focus, and integration settings; the region of interest is chosen away from edges and specular highlights to minimize bias. The emissivity of the propellant is determined by calibrating the camera against a known specimen temperature while accounting for reflected ambient radiation. For opaque surfaces, the indicated temperature depends on both surface emission and reflected environmental radiance. To quantify the reflected contribution, a crumpled aluminum-foil target is placed adjacent to the specimen and imaged with the camera emissivity set to unity. Because the foil is highly reflective in the thermal IR, its indicated temperature is dominated by ambient radiance and is taken as the apparent background temperature. The specimen is then brought to a known temperature by mounting it on a heating pedestal set to 35 °C, covering the assembly with insulation, and allowing approximately one hour for equilibrium. A video recording is initiated, the insulation is removed, and the first frame after removal is analyzed under the assumption of negligible cooling at that instant. With the background temperature fixed from the foil measurement, the camera's emissivity parameter is adjusted until the indicated specimen temperature matches the known value. The emissivity at this match is taken as the band-averaged hemispherical emissivity in the camera's spectral band. Care is taken to maintain identical viewing geometry and ambient conditions during calibration and measurement.

The thermal conductivity k of the solid propellant is measured with a transient hot-point probe. A short power step is applied, the early-time temperature rise is fitted to the probe's calibrated semi-infinite response, and k is extracted.

To determine the interfacial thermal contact conductance, the fixture is driven by a prescribed temperature ramp while the propellant grain's surface temperature is recorded by infrared thermography. Heater power and fixture sensor signals are acquired synchronously with the IR frames under the emissivity-calibrated viewing geometry, providing the dataset required for subsequent inverse identification.

MATHEMATICAL MODEL

The mathematical model mirrors the small-sample experimental configuration used for parameter identification.

The computational domain is $\Omega = \Omega_{sp} \cup \Omega_{Al}$, containing the propellant subdomain Ω_{sp} and the aluminum fixture Ω_{Al} , with internal interface $\Omega_{Al} \cap \Omega_{sp} = \Gamma_I$ over $\tau = [0, t_F]$. Material fields

$$\begin{aligned} \rho(x, T) &= \begin{cases} \rho_{Al} & , (x, t) \in \Omega_{Al} \times \tau \\ \rho_{sp} & , (x, t) \in \Omega_{sp} \times \tau \end{cases} \\ c_p(x, T) &= \begin{cases} c_{p,Al} & , (x, t) \in \Omega_{Al} \times \tau \\ c_{p,sp} & , (x, t) \in \Omega_{sp} \times \tau \end{cases} \\ k(x, T) &= \begin{cases} k_{Al} & , (x, t) \in \Omega_{Al} \times \tau \\ k_{sp} & , (x, t) \in \Omega_{sp} \times \tau \end{cases} \end{aligned}$$

are piecewise constant. Under the assumption that bulk conduction dominates and external convection is negligible relative to radiation in the considered temperature range, the temperature field $T(x, t)$ satisfies on the entire domain

$$\rho c_p \partial_t T - \nabla \cdot (k \nabla T) = 0 \quad \forall (x, t) \in \Omega \times \tau.$$

The initial condition is

$$T(x, t) = T_0(x) \quad \forall (x, t) \in \Omega \times 0.$$

The boundary is partitioned into $\partial\Omega = \Gamma_N \cup \Gamma_D$ with $\Gamma_N \cap \Gamma_D = \emptyset$. Furthermore for known data we assume a Dirichlet boundary (heater-controlled surface) and for the Neumann boundary we assume the classical radiation equation

$$\begin{aligned} T(x, t) &= T_{\Gamma_D}(x, t) & \forall (x, t) \in \Gamma_D \times \tau \\ (-k \nabla T) \cdot n_{\Gamma_N} &= \sigma_{SB} \varepsilon (T^4 - T_\infty^4) & \forall (x, t) \in \Gamma_N \times \tau \end{aligned}$$

with the Stefan-Boltzmann constant σ_{SB} , the band-averaged surface emissivity ε and T_∞ , the ambient radiative temperature. No convective boundary term is included, consistent with the shielded setup.

Imperfect thermal contact at $\Omega_{Al} \cap \Omega_{sp} = \Gamma_I$ is represented by continuity of normal heat flux and a temperature jump proportional to that flux:

$$T_{Al} - T_{sp} = R_c q_{\Gamma_I} \quad \forall (x, t) \in \Gamma_I \times \tau$$

$$k_{Al} \nabla T_{Al} \cdot n_{\partial\Omega_{Al} \cap \Gamma_I} = k_{sp} \nabla T_{Al} \cdot n_{\partial\Omega_{sp} \cap \Gamma_I} = q_{\Gamma_I} \quad \forall (x, t) \in \Gamma_I \times \tau$$

with T_{sp} and T_{Al} denoting the traces on Γ_I from Ω_{sp} and Ω_{Al} , q_{Γ_I} interfacial normal heat flux, and $R_c \geq 0$ the thermal contact resistance. Equivalently

$$h_c (T_{Al} - T_{sp}) = q_{\Gamma_I} \quad \forall (x, t) \in \Omega \times \tau$$

with $h_c = \frac{1}{R_c}$. These conditions capture partial contact and are central to the subsequent inverse identification.

NUMERICAL SETUP

The forward model is discretized with a discontinuous Galerkin (DG) method on a conforming tetrahedral mesh of $\Omega \in \mathbb{R}^3$. The aluminum fixture and the solid propellant are coupled across the internal interface Γ_I . The external boundary is split into Γ_D (heater-controlled Dirichlet) and Γ_N (radiation). Γ_N consists only of the propellant's exterior surfaces; fixture faces are assumed as approximately non-radiative due to insulation. Dirichlet data are imposed strongly on Γ_D .

Let V_h denote the broken polynomial DG space on the mesh. We seek a temperature field T_h with test functions $\varphi_h \in V_h$ and piecewise-constant material fields (ρ, c, k) on Ω_{sp} and Ω_{AL} .

Aluminum (Al) properties are fixed as $\rho_{AL} = 2630 \text{ kg m}^{-3}$, $c_{p,AL} = 960 \text{ J kg}^{-1} \text{ K}^{-1}$, and $k_{AL} = 135 \text{ W m}^{-1} \text{ K}^{-1}$; solid propellant (sp) properties are $\rho_{sp} = 1560 \text{ kg m}^{-3}$, $c_{p,sp} = 1882 \text{ J kg}^{-1} \text{ K}^{-1}$, and $k_{sp} = 0.19 \text{ W m}^{-1} \text{ K}^{-1}$. σ_{SB} is the known Stefan-Boltzmann constant. The ambient radiative temperature is $T_\infty = 295.65 \text{ K}$ (22.5 °C).

The spatial semi-discrete weak form reads

$$m(\partial_t T_h, \varphi_h) + a(T_h, \varphi_h) = l_{\Gamma_D}(\varphi_h) + nl(T_h, \varphi_h) \quad \forall \varphi_h \in V_h$$

with the mass form

$$\sum_K \int_K \rho c_p \partial_t T_h \varphi_h d\Omega =: m(\partial_t T_h, \varphi_h) \quad \forall \varphi_h \in V_h$$

over all Elements K of the Triangulation. The diffusion form

$$a_\Omega(T_h, \varphi_h) + a_{\Gamma_D}(T_h, \varphi_h) + a_{\Lambda/\Gamma_I}(T_h, \varphi_h) + a_{\Gamma_I}(T_h, \varphi_h) =: a(T_h, \varphi_h) \quad \forall \varphi_h \in V_h$$

is constructed with the symmetric interior penalty Galerkin method (SIPG): it combines the volumetric conduction term

$$\sum_K \int_K k \nabla T_h \cdot \nabla \varphi_h \, d\Omega =: a_\Omega(T_h, \varphi_h) \quad \forall \varphi_h \in V_h$$

with consistency and stability terms on the Boundary and mesh skeleton Λ , excluding Γ_I . Jumps and averages across interior faces are defined in the typical way in DG approaches. The penalty parameter γ scales with k , respective the harmonic average $k|_{\Gamma_I} =: k_{eff}$ and the local face size h to ensure coercivity without excessive artificial diffusion. By summing over the corresponding faces, the equations

$$\begin{aligned} \sum_F \int_F \frac{\gamma}{h} k T_h \varphi_h - k \nabla T_h \cdot n_{\Gamma_D} \varphi_h - k T_h \nabla \varphi_h \cdot n_{\Gamma_D} \, d\Gamma_D & =: a_{\Gamma_D}(T_h, \varphi_h) \quad \forall \varphi_h \in V_h \\ \sum_F \int_F \frac{\gamma}{h} k_{eff} [[T_h]] [[\varphi_h]] - \{ \{ k_{eff} \nabla T_h \} \} \cdot [[\varphi_h]] & =: a_\Lambda(T_h, \varphi_h) \quad \forall \varphi_h \in V_h \\ - [[T_h]] \{ \{ k_{eff} \nabla \varphi_h \} \} \, d(\Lambda/\Gamma_I) & \end{aligned}$$

hold.

The imperfect thermal contact across Γ_I is represented by a dedicated interface term

$$\sum_F \int_F h_c [[T_h]] [[\varphi_h]] \, d\Gamma_I =: a_{\Gamma_I}(T_h, \varphi_h) \quad \forall \varphi_h \in V_h,$$

which enforces continuity of normal heat flux while permitting a temperature jump proportional to the interfacial conductance h_c . Nonlinear radiation is applied on Γ_N through the boundary functional

$$\sum_F \int_F \sigma_{SB} \varepsilon (T_h^4 - T_\infty^4) \varphi_h \, d\Gamma_N =: nl(T_h, \varphi_h) \quad \forall \varphi_h \in V_h$$

And known Dirichlet values are inserted, such that

$$\sum_F \int_F \frac{\gamma}{h} k T_{\Gamma_D} \varphi_h - k T_{\Gamma_D} \nabla \varphi_h \cdot n_{\Gamma_D} \, d\Gamma_D =: l_{\Gamma_D}(\varphi_h) \quad \forall \varphi_h \in V_h$$

yields.

Time integration proceeds with a three-stage, fourth order singly diagonally implicit Runge–Kutta (SDIRK) scheme in the spirit of Nørsett. At each stage, the nonlinear residual - comprising the SIPG diffusion, the contact interface term on Γ_I , and the radiation boundary functional on Γ_N - defines a stage equation that is solved by Newton–Raphson iteration. The resulting linearized Jacobian systems are global due to interelement coupling and boundary contributions and are solved with a preconditioned conjugate-gradient method using a Jacobi preconditioner. Strong Dirichlet values on Γ_D are enforced at every stage. The time step Δt is chosen to

resolve the transient response while maintaining robustness of the nonlinear and linear solves. Convergence is monitored through the nonlinear residual norm and the linear relative residual, with damping applied as needed in the early heating transient.

Only the interfacial contact conductance h_c on Γ_N is identified in this work. The inverse problem minimizes the time-accumulated L^2 discrepancy between simulated and measured temperatures on the propellant surface (Γ_N), using an operator that maps model surface temperatures to the infrared camera's region of interest. An L-BFGS optimizer with physically plausible bounds solves

$$\min_{h_c} J(T_h(h_c), T_{exp}) := \min_{h_c} \int_{\tau} \int_{\Gamma_N} (T_{h,sp} - T_{exp,sp})^2 d\Gamma_N d\tau$$

and the gradient $\partial_{h_c} J(T_{sim}(h_c), T_{exp})$ is computed analytically via the adjoint of the semi-discrete DG weak form.

EXPERIMENTAL RESULTS

The transient hot-point test yields a room-temperature thermal conductivity for the solid propellant of $k = 0.19 \text{ W m}^{-1} \text{ K}^{-1}$.

The emissivity tests could successfully be conducted and $\varepsilon = 0.588$ for the solid propellant was identified at an ambient radiative temperature of 295.65 K (Figure 3).

For the ramp experiments, the originally specified cartridge heaters were not available (incorrect units were delivered). To keep the campaign on schedule, thin heating foils were installed as a temporary fallback until the correct cartridge heaters are supplied. The foils' lower thermal inertia and uniform heat input enabled a stable boundary-temperature ramp; with this interim configuration, the fixture executed an approximately linear 5 K increase over 90 s and the procedure was repeatable.

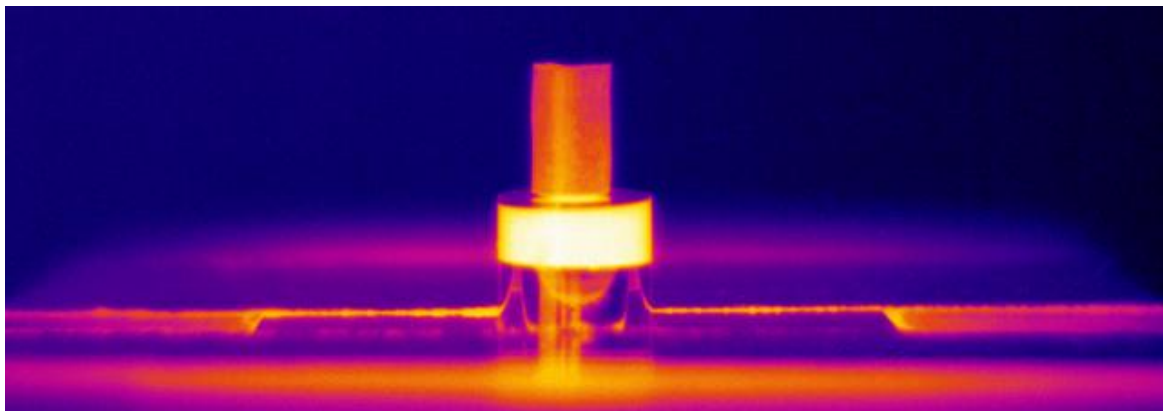


Figure 3: IR Camera Image during the calculation of the emissivity coefficient.

Infrared thermography recorded full-field propellant surface temperatures throughout the ramp (Figure 4) at 1 Hz, currently constrained by the camera's software export function. All IR temperatures were evaluated using the emissivity determined in the setup ($\varepsilon = 0.588$ for the solid propellant). To mitigate frame-to-frame oscillations, the IR fields were post-processed with mild spatial cubic-spline smoothing (third order) and a temporal moving average before analysis (Figure 5). The synchronized fixture and IR measurements constitute the dataset used for the subsequent inverse identification of the interfacial contact conductance h_c .

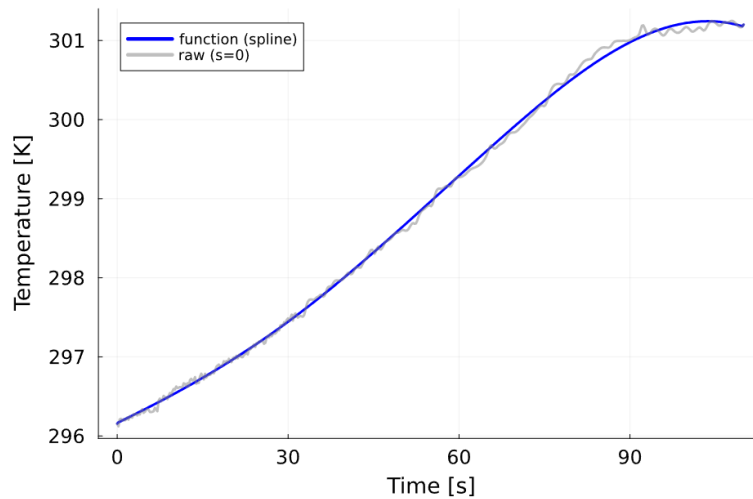


Figure 4: Temperature evolution of the fixture measured by built in sensors.

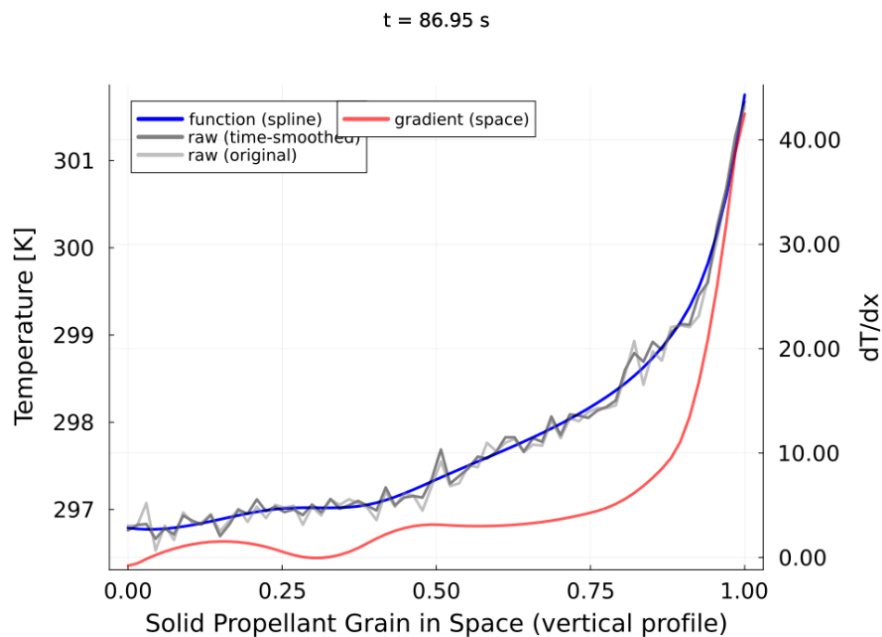


Figure 5: Smoothened vertical profile of the Temperature of the solid propellant grain at $t=87$ seconds.

NUMERICAL RESULTS

The numerical framework was verified against a manufactured analytical solution for the perfect-contact case. Mesh-refinement and polynomial-order studies showed the expected convergence. For the settings used here—first-order DG with a medium mesh and local refinement near the propellant–fixture interface—the maximum error relative to the analytical temperature remained below 0.1%. Production simulations covered the full 90 s boundary-temperature ramp.

Imperfect-contact simulations qualitatively reproduced the measured surface-temperature rise and spatial gradients observed by infrared thermography, consistent with the dominance of radiative losses at the exposed propellant surface and finite heat transfer across the grain–fixture interface (Figure 6). Early-time numerical artifacts were observed when using overly large time steps or too small SIPG penalty parameters. Reducing the time step and increasing the penalty within the stable range eliminated these instabilities without altering the fitted dynamics.

A preliminary sweep of the interfacial contact conductance h_c showed that the objective function is not monotonic in h_c , with a clear minimum near $h_c \approx 10$ for the values tested (Figure 7).

Due to late availability of the final dataset, the adjoint-based L-BFGS optimization was initiated but not completed before submission, and misfit reduction along early iterations was not monotonic. Complete inversion results will be presented in future work and are not included in this manuscript.

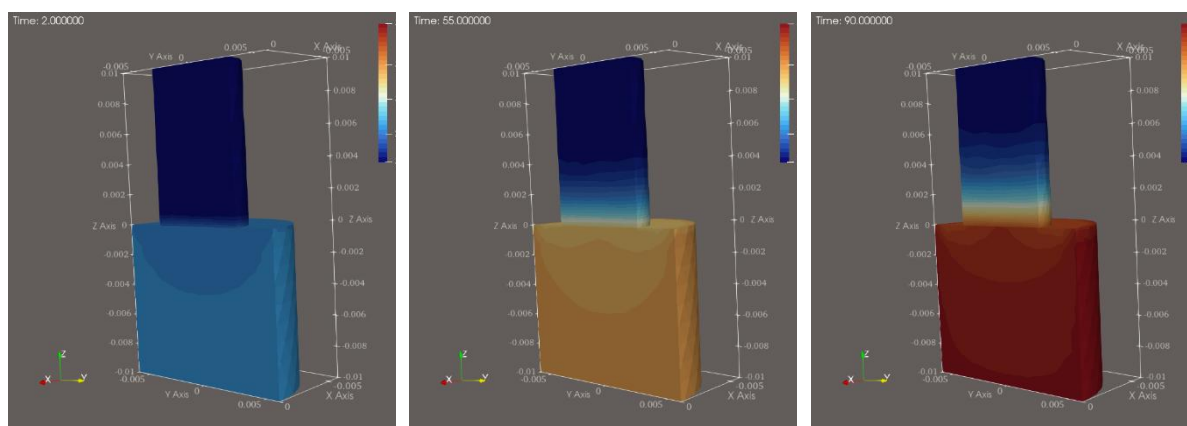


Figure 6: Exemplary Evolution of the Temperature field of the forward simulation using $h_c = 1000$.

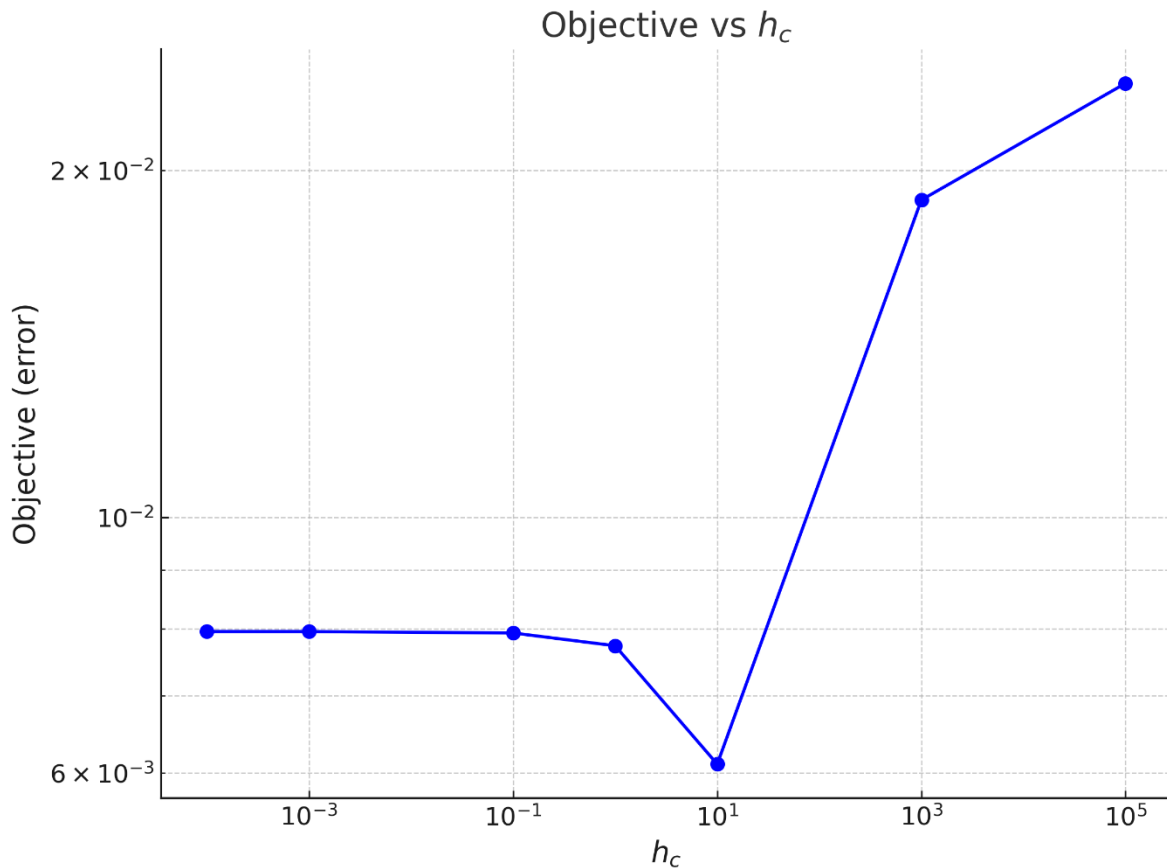


Figure 7: Preliminary sweep of the results of the minimization object by varying interfacial contact conductance h_c .

CONCLUSION AND FUTURE WORK

This work introduced a simulation-based inverse methodology to determine effective thermal parameters of solid propellant from small-sample experiments. The setup combines emissivity-calibrated IR thermography with a controlled heater ramp and a high-fidelity DG solver that incorporates radiative boundary conditions and imperfect thermal contact. The numerical framework was verified against an analytical solution, and forward simulations captured key features of the measured surface-temperature evolution under ramp heating. A preliminary exploration of interfacial conductance confirmed identifiability while revealing a non-monotonic objective landscape across the thermal resistance.

Future work will complete the adjoint-based L-BFGS optimization with the full dataset and report parameter values together with uncertainty estimates and sensitivity analysis. We will increase numerical fidelity by raising the DG polynomial order, further refining the mesh - especially near the interface - and reassessing solver tolerances

for early transients. The inversion will be extended to the propellant's thermal conductivity k and, if warranted, its temperature dependence to ensure consistency between hot-point measurements and forward-model predictions. On the data-processing side, we will try different spatio-temporal smoothing strategies for the IR fields to reduce noise without biasing gradients. Experimentally, we will install the specified cartridge heaters to achieve higher and more precisely controlled thermal gradients, increase IR sampling rate and improve the export/synchronization workflow, and deploy a better housing with an adjustable slot and active temperature control to stabilize the ambient radiative environment and further suppress convection.

References

- [1] "STANAG 4439 (Edition 3): Policy for introduction and assessment of insensitive munitions (IM)," 2010.
- [2] "STANAG 4240 (Edition A, Version 2): Fast heating test procedures for munitions," 2022.
- [3] "STANAG 4382 (Edition A, Version 2): Slow heating test procedures for munitions," 2022.
- [4] D. Tomaschewski, "Modeling and Simulation of Cook-Off Scenarios of DEM - Based Three-Dimensional Propellant Beds in Cased Munitions," in *Energetic Materials Technology Working Group, May 2024, Oslo, Norway*.
- [5] Q. Ye and Y. Yu, "Numerical analysis of cook-off behavior of cluster tubular double-based propellant," *APPL THERM ENG*, vol. 181, 2020, doi: 10.1016/j.applthermaleng.2020.115972.
- [6] H. Sahin, B. Narin, and D. F. Kurtulus, "Development of a Design Methodology Against Fast Cook-Off Threat for Insensitive Munitions," *PROPELL EXPLOS PYROT*, vol. 41, no. 3, 2016. doi: 10.1002/prop.201500333. [Online]. Available: 587
- [7] H. Isik and F. Goktas, "Cook-off analysis of a propellant in a 7.62 mm barrel by experimental and numerical methods," *APPL THERM ENG*, vol. 112, 2017. doi: 10.1016/j.applthermaleng.2016.10.104. [Online]. Available: 496
- [8] M. L. Gross, T. D. Hedman, and K. V. Meredith, "Considerations for Fast Cook-Off Simulations," *PROPELL EXPLOS PYROT*, vol. 41, no. 6, pp. 1036–1043, 2016, doi: 10.1002/prop.201500253.
- [9] M. Graswald, R. Gutser, and M. Schweizer, "Extended multi-physics model for slow-cook off events of warheads," in *Insensitive Munitions and Energetic Materials Technology Symposium. Seville, Spain, 2019*.